Mem. S.A.It. Vol. 79, 1178

Memorie della

The X-Ray view of AGN ionized outflows

F. Nicastro[1,2,3], Y. Krongold[4], and M. Elvis[3]

[1] Istituto Nazionale di Astrofisica – Osservatorio Astronomico di Roma, Via Frascati 33, I-00040 Monteporzio Catone (RM), Italy, e-mail: fnicastro@oa-roma.inaf.it
[2] IESL, FORTH-Hellas, 71 110, Voutes, Heraklion, Crete, Greece
[3] Harvard-Smithsonian Center for Astrophysics, Cambridge, MA 02138, USA
[4] Universidad Nacional Autonoma de Mexico, Mexico City, DF, Mexico

Abstract. We present time-resolved X-ray spectra of AGN ionized outflows, and discuss the power of time-evolving photoionization as a diagnostic tool to measure the electron density of photoionized gas. We apply this technique to a XMM-*Newton* observation of the ionized absorber in the small black hole mass, low luminosity, Narrow Line Seyfert 1 galaxy NGC 4051, and a Suzaku monitoring campaign of the prototypical Seyfert 1 galaxy NGC 5548, and present the first measurements of the ionized absorber volume density, its distance from the central ionizing source, and so its mass outflow rate, in these two sources. By extrapolating these measurements to high-luminosity, large black hole mass, quasars, we speculate that AGN winds can play important roles both in the AGN-host-galaxy and AGN-IGM feedback processes.

Key words. AGN: outflows –AGN: Warm Absorbers – AGN: Narrow Absorption Line objects – Galaxy: feedback –IGM: feedback

1. Introduction

Ionized X-ray (*Warm Absorbers*: WAs) and UV (*narrow Absorption Lines*: NALs) outflow ($v_{out} \simeq 500-5000$ km s^{-1}) absorbers have been observed in the spectra of $\gtrsim 50$ % of Seyfert 1s (e.g. Crenshaw et al. 2003; Kriss 2004) and quasars (Piconcelli et al. 2005; Misawa et al., 2007). Such high detection rates, combined with evidence for transverse flows (e.g. Mathur et al. 2005; Crenshaw et al. 2003), suggest that WAs/NALs are actually ubiquitous in AGN, but become directly visible in absorption only when our line of sight crosses the outflowing material. Despite their ubiquity, very little is still know about their physical state, dynamical strength and geometry. The most fundamental question is where do quasar winds originate? Proposed locations span a range of 10^6 in radial distance from the central source, from the innermost radii of the accretion disk, to the Broad Emission Line Region, the molecular torus, all the way out to the Narrow Emission Line Regions. Several important astrophysical quantities, like the mass outflow rate and the total outflow kinetic energy, depend critically on the exact location of these outflows with respect to the central ionizing source: farther the base of outflow from the central ionizing source, larger the mass outflow rate and the total available outflow kinetic power. Addressing this question is therefore extremely important, and carries cosmological

Send offprint requests to: F. Nicastro

implications, such as the importance of AGN outflows for AGN-galaxy and AGN-IGM feedback mechanisms.

Measuring the AGN ionized outflow location, however, requires the independent determination of a quantity which is not directly observable: the electron density n_e of the outflowing material. Here we show that a powerful way of determining the electron density n_e of gas photoionized by variable ionizing radiation, is to follow the evolution in time of the ionization degree of the gas and modeling it with time-evolving photoionization models. We apply this technique to: (a) a high S/N XMM-*Newton* observation of the low luminosity ($L_{bol} = 2.5 \times 10^{43}$ ergs s^{-1}, Ogle et al. 2004), low black hole mass ($M_{BH} = 1.9 \times 10^6$ $M_\odot$, Peterson et al. 2004), and rapidly ($\sim$ 1 hour) and highly (factor of $\sim$ 10, McHardy et al. 2004) X-ray variable Narrow Line Seyfert 1 NGC 4051, and (b) to a 1.5 month *Suzaku* monitoring campaign of the prototypical Seyfert 1 galaxy NGC 5548.

2. Time evolving photoionization

Recent studies have mostly shown that WAs are made up of just a few distinct physical components (e.g. Krongold et al., 2007, - K07 - and reference therein). However, for each of these components, only average estimates of the product ($n_e R^2$) could be derived, from time-averaged spectral analyses. This is due to the intrinsic degeneracy of n_e and R in the equation that defines the two observables: the ionization parameter of the gas $U_x = Q_x/(4\pi R^2 c n_e)$ and the luminosity of ionizing photons Q_x.

An unambiguous method to remove this degeneracy is to monitor the response of the ionization state of the gas in the wind to changes of the ionizing continuum (Krolik & Kriss 1995; Nicastro et al. 1999: hereinafter N99). Time-evolving photoionization equations define the Photoionization Equilibrium Time scale, t_{eq}, that measures the time necessary for the gas to reach photoionization equilibrium with the ionizing continuum (N99). In a 3-ion only approximation, and considering only photoionization and radiative recombination, the equilibration time-scale for the ion i of the element X, at any point of the light curve of the ionizing continuum, can be written:

$$t_{eq}^{X^i,X^{i+1}}(t \rightarrow t+\delta t) \sim \left[\frac{1}{\alpha_{rec}(X^i,T_e)n_e}\right] \times \left\{\frac{1}{[\alpha_{rec}(X^{i-1},T_e)/\alpha_{rec}(X^i,T_e)]_{eq} + (n_{X^{i+1}}/n_{X^i})_{eq}}\right\}_{t+\delta t}, \quad (1)$$

where n_{X^i} is the relative ionization fraction of the ion X^i, $\alpha_{rec}(X^i,T_e)$ is the radiative recombination coefficient for the ion X^i at an electronic temperature T_e, n_e is the gas electronic density, and *eq* indicates equilibrium quantities. This time-scale depends explicitly on the electron density n_e in the cloud, during both increasing and decreasing ionizing continuum phases (N99). Non-equilibrium photoionization models can therefore be used to measure the density of the gas n_e and, hence, its distance from the ionizing source.

3. The variable ionized absorber of NGC 4051

NGC 4051 was observed for ~117 ks with the XMM-Newton Observatory, on 2001 May 16-17. The source varied by a factor of a few on timescales as short as 1 ks, and by a factor of ~12 from minimum to maximum flux over the whole observation (Fig. 1a). Details of the data reduction and analysis can be found in K07.

Two physically distinct but dynamically coincident ($v_{out} = 500$ km s^{-1}) WA phases were found in the average RGS spectrum of NGC 4051: a high- and a low-ionization phase (HIP and LIP).

3.1. Following the time variability of HIP and LIP

To study the response of the WAs of NGC 4051 to ionizing flux changes, we performed a time-resolved spectral analysis of 21 EPIC-PN spectra extracted from 21 distinct continuum lev-

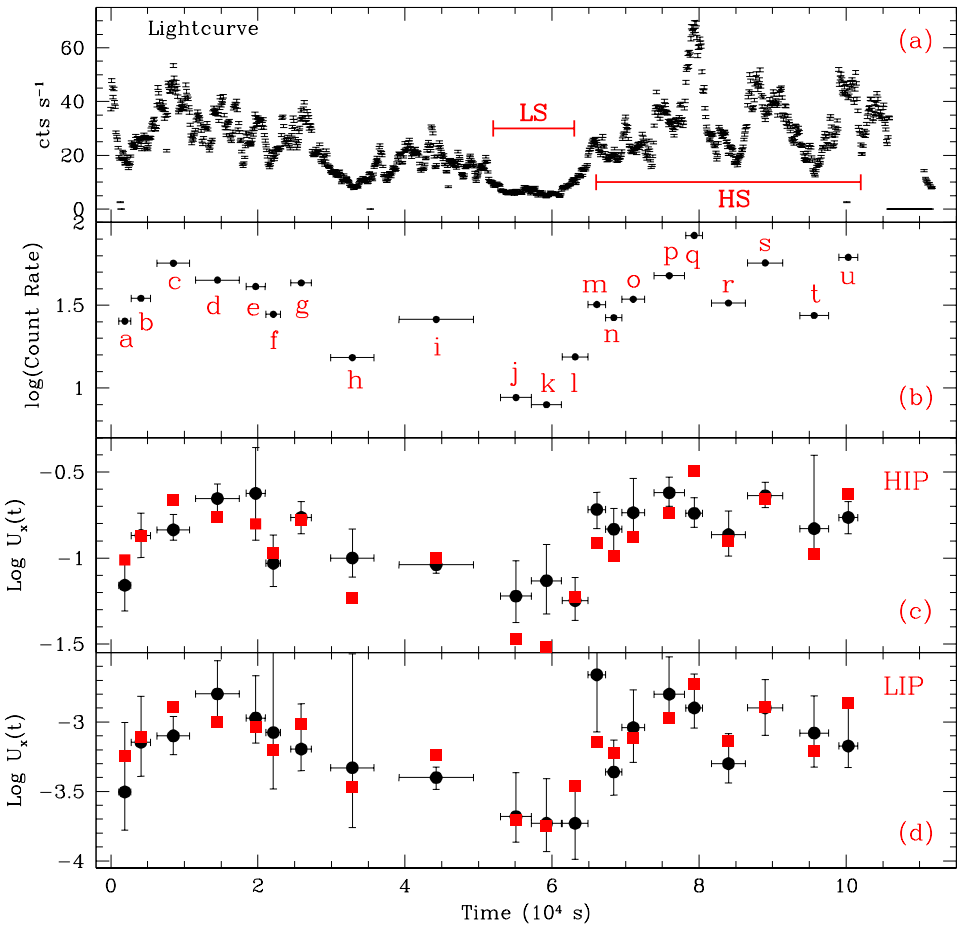

Fig. 1. Lightcurve of NGC 4051 in bins of 100 s [panel (a)]; Log of the count rate vs. time, for the 21 "flux states" used in this analysis [panel (b)]; Log of the ionization parameter of HIP [panel (c)] and LIP [panel (d)] as a function of time: filled squares are the expected value of U_X at equilibrium.

els (*a* - *u*, see Fig. 1b) [1] . For both absorbing components the derived U_X values follow closely the source continuum lightcurve [compare panel (c) and (d) with panel (b) of Fig. 1], clearly indicating that the gas is responding quickly to the changes in the ionizing continuum.

To study more quantitatively how these changes are related to the changes in the continuum, we show in Fig. 2a,b the log of the source count rate ($\log C(t)$) vs. $\log U_X(t)$, for the HIP [panel (a)] and the LIP [panel (b)]. For most of the points of the HIP and for all the points of the LIP (within 2σ), $\log C(t)$ correlates with $\log U_X(t)$ tightly, which allows us to

[1] We checked, on average Low- and High-State (LS and HS in Fig. 1a) RGS and EPIC-PN spectra, that both detectors allowed the detection of WA opacity variations, and gave consistent results (see K07)

derive robust estimates of the quantity ($n_e R^2$) for both components (best fit lines in Fig. 2a,b, Table 1).

Fig. 2a,b shows that the LIP is always in photoionization equilibrium with the ionizing flux, while the HIP deviates from photoionization equilibrium during periods of extreme flux states. Unlike the LIP, then (for which only an upper limit on t_{eq}, and so a lower limit on n_e, can be estimated), the behavior of the HIP allows us to set both lower and upper limits on $t_{eq}(HIP)$, and so on $n_e(HIP)$.

4. The non-variable ionized absorber of NGC 5548

NGC 5548 underwent a ∼ 2 month long monitoring campaign with the *Suzaku* observatory in 2007, with weekly visits of 40 ksec each. The source varied by a factor of ∼ 4 during this campaign on a timescale of ∼ 10 days Fig. 3a). Details of the data reduction and analysis can be found in Krongold et al., 2008 (in preparation).

The *Suzaku* CCD detectors have good spectral resolution at low energy, but not sufficient to identify the number of physically and/or kinematically distinguished warm absorber components present in the nuclear environment of an AGN. Superior grating spectral resolution are needed. For such reason we retrieved and analyzed two long (800 ksec total) *Chandra* HETG and LETG archival observations of NGC 5548, and modeled the data with our Photoionized Absorber Spectral Engine (*Phase*, Krongold et al., 2003) code. We found that two kinematically distinguished WA components were present in these *Chandra* spectra, with outflow velocities of ∼ 500 km s^{-1} (hereinafter Low Velocity - LV - component) and ∼ 1100 km s^{-1} (hereinafter High Velocity - HV - component). Each of these two kinematically distinct components, were modeled with two physically distinct phases: a Low Ionization phase (LIP) and a high Ionization phase (HIP), for the LV component, and a HIP and a Super-High Ionization phase (SHIP), for the HV component. The SHIP For both the LV and the HV components, the physically distinct phases are consistent with beig in pressure equilibrium, and so possibly co-located.

Fig. 3b,c,d shows the log of the source count rate (log$C(t)$) vs. log$U_X(t)$, for the SHIP [panel (b)], the HIP [panel (c)] and the LIP [panel (d)]. Clearly the SHIP does not respond to the ionizing radiation variations, and appear always over-ionized with respect to the equilibrium ionization states. This is expected for gas with electron densities such that the photoionization equilibration time during recom-

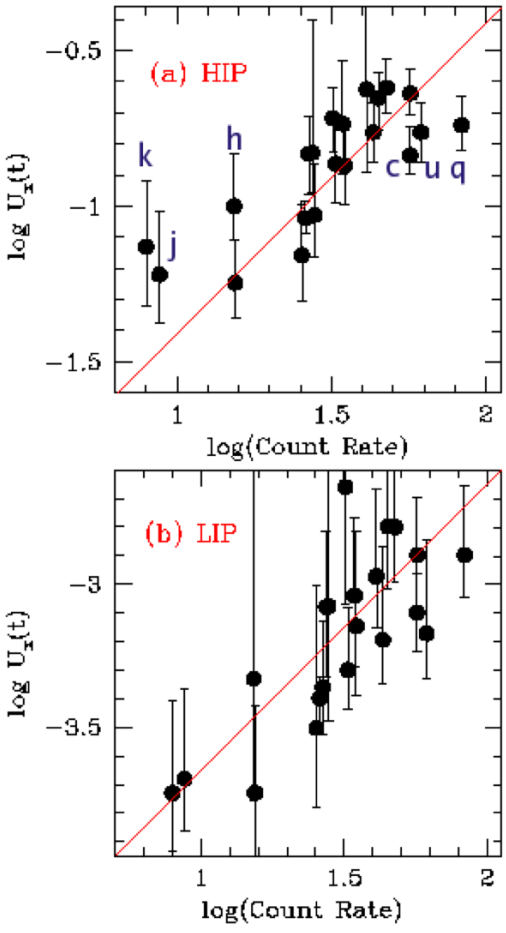

Fig. 2. Log$U_X(t)$ vs. log of the source count rate for the HIP [panel (a)] and the LIP [panel (b)].

Table 1. Physical and dynamical parameters of HIP and LIP of NGC 4051

Abs.	$(n_e R^2)$	n_e	P_e	R	ΔR	$(\Delta R/R)$	$\dot{M}_{out}/\dot{M}_{in}$
	10^{38} cm^{-1}	10^7 cm^{-3}	10^{12} K cm^{-3}	10^{15} cm	10^{14} cm		%
			NGC 4051				
HIP	(0.38 ± 0.05)	(0.58-2.1)	(2.9-10.5)	(1.3-2.6)	(1.9-7.2)	(0.1-0.2)	(2-3)
LIP	(66 ± 3)	> 8.1	> 2.4	< 8.9	< 0.09	$< 10^{-3}$	< 2
			NGC 5548				
SHIP	(... ± ...)	< 0.054	(...)	$> 6.2 \times 10^5$	(...)	(...)	> 2.5

bination is much longer than the typical variability timescale $\sim$ 1 week). For the other 2 phases, HIP and LIP, the data are noisier than for the SHIP and no clear conclusion can be drawn, although both components are consistent with being constant in ionization degree and possibly in equilibrium with the average ionizing source flux. From such data, therefore, only an upper limit to the electron density of the SHIP (that carries most of the mass) can be derived.

5. Results

From the independent estimates of n_e and $(n_e R^2)$ for the LIP and HIP of NGC 4051, and for the SHIP of NGC 5548, we can derive limits on R and so evaluate all physical and dynamical parameters of the gas, including the mass outflow rate. Table 1 summarizes our findings. Fig. 4 shows a schematic view of the location of the ionized outflow in NGC 4051. We find that:

(1) time-evolving photoionization models are key diagnostics to measure the electron density in gas photoionized by variable X-ray sources;
(2) the two X-ray WA components of NGC 4051 are both close to photoionization equilibrium, dense, compact and possibly in pressure balance (Fig. 4, Table 1);
(3) the Narrow Emission Line Region (NELR), molecular torus and any radial continuous flow, are all ruled out as origin of the WAs of NGC 4051 (Fig. 3);
(4) a static spherical configuration for the WAs of NGC 4051 is ruled out, and a dynamical but stationary spherical configuration (i.e. expulsion of thin spherical shells at regular time intervals) is highly unlikely, since it requires extremely fine tuning not to degenerate in a radial continuous flow;
(5) the next simplest geometrical configuration, for the WAs of NGC 4051, is that of geometrically thin cone sections, originating in the accretion disk at a distance consistent with that of the high-ionization BLRs (Fig. 3; Elvis, 2000);
(6) if this configuration applies to all AGN, then the presence or absence of WAs in the X-ray spectra of type 1 AGNs is explained simply by orientation, with WAs being visible only in those objects seen between edge-on and an angle equal to the disk-outflow angle;
(7) in the framework of such empty bi-cone configuration we estimate an outflow rate for the WA of NGC 4051, which is only 2-5% of the inner accretion rate. By assuming that all the Black Hole mass of NGC 4051 (M_{BH}(NGC 4051) = 2×10^6 $M_\odot$) has been accreted at the current inner accretion rate, this gives a total mass available to be deployed into the ISM/IGM of only $(0.4 - 1) \times 10^5$ $M_\odot$, only a small fraction of the mass that can potentially be deployed by powerful Ultraluminous Infrared Galaxy (ULIRG) super-winds (up to $\sim 10^8$ $M_\odot$), and so unimportant for both ISM and IGM enrichment. Similarly the total available kinetic energy from the ionized outflows of NGC 4051 is $E_K \simeq (0.4-1) \times 10^{53}$ ergs, $\sim$ 1% the $\sim 10^{55}$ ergs required to unbound the hot ISM components and inhibit star formation (e.g. Hoptkins et al., 2006) and a negligible fraction of the $\sim 10^{60}$ ergs required to control the host-galaxy and sur-

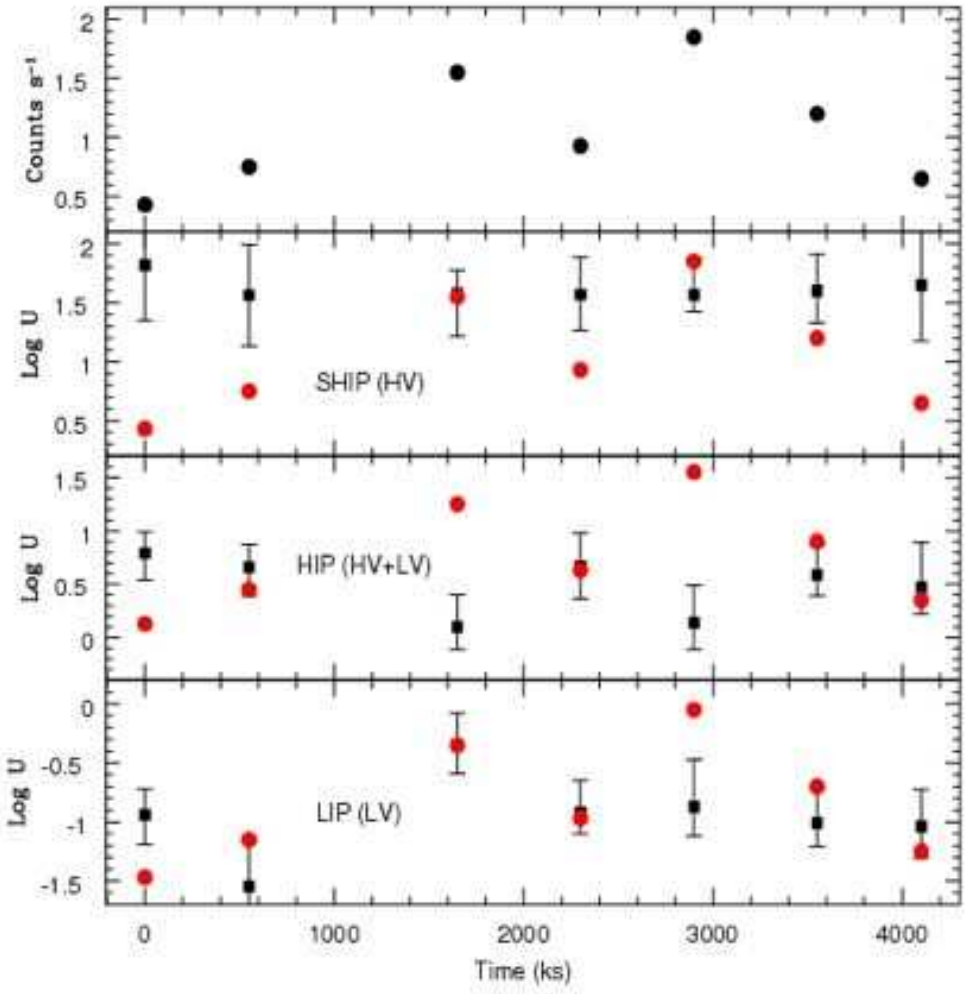

Fig. 3. Lightcurve of NGC 5548 in bins of 40 ksec [top panel (a)]; Log of the ionization parameter of the SHIP [HV component only, second panel from top (b)], the HIP [HV plus LV components, third panel from top (c)], and the LIP [LV component only, bottom panel (d)], as a function of time: red circles are the expected value of U_X at equilibrium.

rounding IGM evolution (e.g. Nataraian et al., 2006);

(8) the situation for the ionized outflow components of NGC 5548 is dramatically different. The data are consistent with the absorbers not responding to the ionizing continuum changes on a timescale of $\sim$ 2 months, which locates the outflows much farther out compared with those of NGC 4051 (Table 1). In the same empty-bi-cone geometry inferred for NGC 4051, this also implies much larger mass outflow rate and kinetic power (Table 1). For the SHIP, we estimate: $\dot{M}_{out} \gtrsim 2.5 \times \dot{M}_{in}$, and so by assuming that all the black hole mass

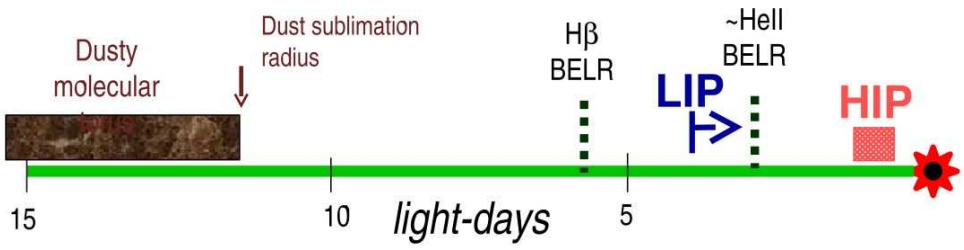

Fig. 4. Location of features in the nuclear environment of NGC 4051 on a light-day scale.

of NGC 5548 has been accreted at the current inner rate, a total mass available to be deployed into the ISM and/or surrounding IGM $M_{av} \gtrsim 1.8{\times}10^8$ $M_\odot$. This is comparable to the one available from the most powerful ULIRG, and thus, in principle able to significantly contribute to the enrichment of the surrounding IGM. Similarly, the total kinetic energy available from the SHIP of NGC 5548 is $E_K \geq 3.3 \times 10^{57}$ ergs, definitely sufficient to unbound the host galaxy hot ISM, and to inhibit large scale star formation, and potentially sufficient to influence both host-galaxy and surrounding IGM evolution.

(9) these values, if extrapolated to high luminosity, massive ($M_{BH} \sim 10^9$ $M_\odot$) QSOs, suggest that WAs may play an important role in locally feeding the IGM with enriched material, and in controlling both AGN-host galaxy and AGN-IGM feedback processes.

Acknowledgements. F.N. acknowledges support by NASA grant NNG05GK47G.

References

Crenshaw, D. M., Kraemer, S. B., & George, I. M. 2003, A&A Rev., 41, 117

Piconcelli, E. et al. 2005, A&A, 432, 15

Mathur, S., Elvis, M., & Wilkes, B. 1995, ApJ, 452, 230

Kriss, G. A. 2004, Proceedings of IAU Symposium, No. 222. Edited by T. Storchi-Bergmann, L.C. Ho, and Henrique R. Schmitt. Cambridge, UK: Cambridge University Press, p.223-228, 265, 87

Misawa, T. et al. 2007, ApJS, 171, 1

Krongold, Y. et al. 2007, ApJ, 659, 1022

Krolik, J. H. & Kriss, G. A. 2001, ApJ, 561, 684

Nicastro, F., Fiore, F., & Matt, G. 1999, ApJ, 517, 108

McHardy, I. M., et al. 2004, MNRAS, 348, 783

Ogle, P. M. et al. 2004, ApJ, 606, 151

Peterson B.M. et al. 2004, ApJ 613, 682